Jeon et al. *NPG Asia Materials* (2023) 15:68
https://doi.org/10.1038/s41427-023-00519-3

NPG Asia Materials

ARTICLE Open Access

Two-dimensional directed lamellar assembly in silicon- and fluorine-containing block copolymer with identical surface energies

Seungbae Jeon[1], Seungjae Lee[1], Junsu Kim[1], Sungoh Eim[1], Wooseop Lee[2], Woo Hyun Nam[3,4], Jeong Gon Son[3,4] and Du Yeol Ryu[1]

Abstract

A block copolymer (BCP) with specific monomer structures of fluoroacrylate polymers was designed by exploiting the inorganic superhydrophobicity and low glass transition temperature of polydimethylsiloxane (PDMS). With the use of a fluorine-containing block providing a surface tension as low as that of PDMS ($19.9 < \gamma < 21.5$ mN/m), PDMS-*b*-poly(2,2,3,3,3-pentafluoropropyl acrylate) (PDMS-*b*-PPeFPA) copolymer was synthesized to create a volume-symmetric lamellar structure. The compositional randomness of the BCP chains adsorbed onto the substrates provided well-balanced interfacial interactions toward the overlaid PDMS-*b*-PPeFPA ($\gamma_{PDMS\text{-}ads} \approx \gamma_{PPeFPA\text{-}ads}$). Under this symmetric confinement with simultaneous dual neutral interfaces, lamellar microdomains with a sub-10 nm half-pitch feature size were successfully oriented perpendicular to the interfaces at room temperature. We showed the response of the BCP films to a lateral electric field, demonstrating that the perpendicular lamellae were adaptively aligned along the electric vector within a short treatment period. Furthermore, the PDMS-*b*-PPeFPA system exhibited a remarkable etch contrast for O_2 reactive ion etching, yielding unidirectionally aligned air–inorganic nanoarrays emanating from the perpendicular lamellae between the electrodes. This study reports a system engineering approach for conceiving highly immiscible, silicon- and fluorine-containing BCP whose components exhibit identical surface tensions ($\gamma_{PDMS} \approx \gamma_{PPeFPA}$) and for generating perpendicularly oriented lamellar microdomains due to substrate neutrality.

Introduction

Nanotechnology, a critical research field focused on nanometer-scale systems, has been advancing in accordance with Moore's law over the past few decades[1]. However, it remains at an intermediate stage in terms of resolving the limitations of the top-down approach in fabricating sub-10 nm feature sizes, which significantly impacts both academic and industrial fields[2]. Directed self-assembly of block copolymers (BCPs) has attracted considerable attention for the miniaturization and multiplication of nanopatterns, thereby enabling low-cost, high-throughput processes in manufacturing[3–8]. In the bottom-up approach to BCP self-assembly, the microdomain orientation of nanostructures with sub-10 nm feature sizes is vital for realizing high-density addressable arrays intended for storage media[9,10]. In particular, BCP systems with a high Flory–Huggins interaction parameter (or high χ value) and small number of segments (or small N value) have been investigated to accommodate feature size reduction under the optimal segregation power (i.e., $\chi N \gg 10.5$)[11,12].

Silicon-, hydroxy-, and fluorine-containing units linked to conventional styrenic or (meth)acrylic units have been introduced into building block structures to increase the immiscibility (or χ value) between two blocks[13–17]. However, most high-χ and low-N BCPs possess a large

Correspondence: Du Yeol Ryu (dyryu@yonsei.ac.kr)
[1]Department of Chemical and Biomolecular Engineering, Yonsei University, 50 Yonsei-ro, Seodaemun-gu, Seoul 03722, Korea
[2]Synchrotron Application Team, Pohang Accelerator Laboratory, 80 Jigok-ro, Nam-gu, Pohang 37673, Korea
Full list of author information is available at the end of the article

surface-energy contrast arising from the different chemical identities, causing preferential wetting onto the substrate and/or surface interfaces[18]. To address this drawback concerning orientation control, several substrate modification strategies have been proposed for orthogonalizing lamellae and cylinders, such as neutral layer methods using copolymers and physically adsorbed layer methods with the BCP itself[19–21]. Interestingly, polarity-switchable, top-coat random copolymers have also been proposed to provide surface neutrality for perpendicular lamellae in high-χ BCP films[22]. Later, neutral top-coat layering approaches using an initiated chemical vapor deposition and plasma oxidization have been introduced[23,24]. Recently, a filtered Ar plasma treatment has been utilized for obtaining neutral top and/or bottom layers using various BCPs[25].

Another challenge is to unidirectionally arrange the perpendicular lamellae or parallel cylinders along the desired direction. To this end, the application of lamellae and cylinders onto grapho- and chemo-epitaxial patterns provides a remarkable multiplication of nanoarrays aligned along micrometer-scale prepatterns[26]. A highly ordered, single-grain nanopattern was achieved by a shear-rolling method combined with the filtered plasma treatment, leading to unidirectional alignment of perpendicular lamellae across a 4-in diameter wafer within 1 min[27]. Moreover, the electric field (E-field) has been utilized to obtain uniaxially aligned, defect-free nanoarrays along the electric vector; this orientational fidelity is favorable for BCP systems with high dielectric anisotropy between the two blocks[28–37].

Reactive ion etching (RIE) has been extensively used to selectively remove one block while retaining or modifying the other block[38,39]. In most BCPs consisting of organic components, the etch contrast between the two blocks is inherently low. However, inorganic–organic hybrid BCPs with a silicon-containing block exhibit a high etch contrast because the silanol groups formed during O_2 RIE are resistant to further destructive etching. For example, inorganic nanotemplates fabricated from polystyrene-*b*-polydimethylsiloxane (PS-*b*-PDMS) exhibit a remarkable nanolithographic performance, highlighting their applicability as etch masks for pattern transfer[40].

In this study, a high-χ, low-N, silicon- and fluorine-containing BCP was explored. To avoid the air preference of one block, we designed specific monomer structures of fluoroacrylate polymers with a surface tension as low as that of PDMS ($\gamma = 21.1$ mN/m). For this purpose, an inorganic–organic BCP, PDMS-*b*-poly(2,2,3,3,3-pentafluoropropyl acrylate) (PDMS-*b*-PPeFPA), was selected and synthesized to create a volume-symmetric lamellar structure with a sub-10 nm half-pitch feature size. The related challenges were addressed by ensuring (1) identical surface tension values of the two blocks ($\gamma_{PDMS} \approx \gamma_{PPeFPA}$) and (2) substrate neutrality arising from a physically adsorbed layer ($\gamma_{PDMS\text{-}ads} \approx \gamma_{PPeFPA\text{-}ads}$). Symmetric confinement with dual neutral interfaces for the BCP films successfully yielded lamellar microdomains oriented perpendicular to the interfaces. The obtained PDMS-*b*-PPeFPA system was then subjected to a lateral E-field (25 V/μm) to investigate the directed alignment of perpendicular lamellae. A remarkable etch characteristic of the PDMS-*b*-PPeFPA system for O_2 RIE enabled the production of unidirectional alignment of the perpendicular air–inorganic (oxidized PDMS) lamellae.

Materials and methods

Synthesis of the PDMS macroinitiator, PDMS-*b*-PPeFPA, and fluoroacrylate homopolymers

A macroinitiator of PDMS-Br and PDMS-*b*-PPeFPA was prepared in a manner similar to that previously reported[41]. Briefly, HO-terminated PDMS (5 mL, 1 mmol) and triethylamine (0.7 mL, 5 mmol) were dissolved in anhydrous tetrahydrofuran (50 mL), and 2-bromoisobutyryl bromide (0.4 mL, 3.0 mmol) was added dropwise to the solution. After purification of the mixed solution, PDMS-Br was obtained and further dried at 50 °C under vacuum for 1 d. PDMS-*b*-PPeFPA copolymer was synthesized *via* atom transfer radical polymerization (ATRP) of PeFPA monomers (99%, Oakwood Chemical) to design a volume-symmetric composition. PDMS-Br (1 mL, 0.2 mmol), degassed PeFPA (5 mL, 40 mmol), *N*,*N*,*N*′,*N*″,*N*″-pentamethyldiethylenetriamine (PMDETA; 84 μL, 0.4 mmol), and copper(I) bromide (CuBr; 0.03 g, 0.2 mmol) were mixed with toluene (5 mL) in a purified Ar environment. After the ATRP reaction (performed at 85 °C for 48 h), the product solution was passed through a neutral alumina-packed column and precipitated in cold methanol three times. The final product was dried at 50 °C under vacuum for 1 d.

Fluoroacrylate homopolymers poly(2,2,2-trifluoroethyl acrylate) (PTFEA), poly(2,2,3,3,3-pentafluoropropyl acrylate) (PPeFPA), and poly(2,2,3,3,4,4,4-heptafluorobutyl acrylate) (PHepFBA) were obtained *via* transesterification of a poly(*tert*-butyl acrylate) (P*t*BA; with a number-averaged molar mass (M_n) of 37,000 Da, Polymer Source) precursor with 2,2,2-trifluoroethanol (99 + %, Oakwood Chemical), 2,2,3,3,3-pentafluoropropanol (98%, Oakwood Chemical), and 2,2,3,3,4,4,4-heptafluorobutanol (97%, Oakwood Chemical), respectively, following a method similar to that previously reported[16]. The conversion was calculated by ^{1}H NMR spectroscopy in a $CDCl_3$ solution.

Thin film preparation

Various substrates, such as a standard Si substrate with a 2 nm-thick native oxide layer, H-passivated Si substrate, and physically adsorbed layer, were fabricated to identify the microdomain orientation of the self-assembled

nanostructure in the BCP films. To prepare the H-passivated Si substrate, a standard Si substrate with a 2 nm-thick native oxide layer was immersed in an aqueous HF solution (5 vol%) for 30 min and then sequentially rinsed with ethanol and deionized (DI) water. To obtain the adsorbed layers, a PDMS-*b*-PPeFPA solution (1.0 wt% in *n*-heptane) was spin-coated onto the H-passivated Si substrate. Then, 30 nm-thick films were annealed at room temperature (RT), which is above the glass transition temperatures (T_gs) of the PDMS and PPeFPA blocks. The films were subsequently immersed in *n*-heptane for 1 d to eliminate any unadsorbed chains, yielding irreversibly adsorbed (~4 nm-thick) layers. The PDMS-*b*-PPeFPA films were supported on various substrates by spin-coating the polymer solution in *n*-heptane. The solution concentration was adjusted between 1.0 and 2.0 wt%, and a spin rate between 2000 and 6000 rpm was employed to fine-tune the film thickness. The BCP films were annealed at RT under vacuum for 1 d. For E-field alignment, adhesive Ti (~5-nm thick) and Au layers (~90-nm thick) were deposited onto a specific Si substrate with a 300-nm thick oxide layer, enabling the fabrication of a pair of 1-mm-long parallel electrodes with a 2 μm-sized gap.

Measurements and characterization

M_n and the volume fraction of the PPeFPA block (f_{PPeFPA}) were determined by ^{1}H nuclear magnetic resonance spectroscopy (^{1}H NMR; Avance II, Bruker) in $CDCl_3$, and the molecular weight distribution ($Đ = M_w/M_n$) was characterized by size exclusion chromatography (SEC; Young Lin Acme 9000) in toluene using PS standards. T_g of the PPeFPA block was measured by differential scanning calorimetry (DSC; PerkinElmer Diamond) using 10-mg BCP samples at a heating rate of 30 °C/min from −70 to 250 °C under N_2 flow. Small-angle X-ray scattering (SAXS) experiments were performed at the 4 C beamline of the Pohang Accelerator Laboratory (PAL), Korea. The operating conditions were as follows: wavelength λ: 1.24 Å; sample-to-detector distance (SDD): 3 m; and exposure time: 1–5 s. The specimen for the heating experiments was sealed in a brass template, and the sample temperature was increased at a heating rate of 1.0 °C/min in an N_2 environment to prevent thermal degradation. Transmission electron microscopy (TEM; JEM-F200, JEOL) was performed at an accelerating voltage of 200 kV to examine the bulk morphology of the BCP. A 60 nm-thick specimen was prepared using a cryo-ultramicrotome (Powertome, RMC) at −150 °C. No specific staining was needed because of the high contrast in the electron density between the two blocks.

The film thickness was evaluated by spectroscopic ellipsometry (MG-1000, Nano-view) at an incident angle of 70.1°. Static contact angle (CA) measurements (Phoenix 300, SEO) were performed to validate the γ values of the homopolymers using DI water and ethylene glycol. Scanning force microscopy (SFM; Dimension 3100, Digital Instruments) was operated in a tapping mode using a probe with a sub-5 nm tip radius (ACTA-SS, AppNano). Field-emission scanning electron microscopy (FE-SEM; 7610F-Plus, JEOL) was conducted at an accelerating voltage of 2.0 kV. Grazing incidence SAXS (GISAXS) experiments were performed at the 9 A beamline of the PAL to analyze the film structures under the conditions of $\lambda = 1.12$ Å and SDD = 6.5–2.5 m. The incidence angle (α_i) was varied from 0.08° to 0.14° across the critical angle (0.109°) of the PDMS-*b*-PPeFPA films. Two-dimensional (2D) GISAXS patterns were recorded using a detector positioned at the end of a vacuum guide tube with an exposure time of 5 s. The RIE experimental conditions (CUTE, Femto Science) were optimized with O_2 (10 sccm) at a radio frequency (RF) power of 100 W to etch the organic PPeFPA block down, producing air–inorganic (oxidized PDMS) nanotemplates.

Results and discussion

Hydrophobic fluorine-containing acrylate polymers—PTFEA, PPeFPA, and PHepFBA, which successively contain more fluorine atoms in each side unit—were first considered in this study because their surface tension values were expected to be as low as that of PDMS ($19.9 < \gamma < 21.5$ mN/m[42]; Fig. 1). The γ values at the polymer–air interface, calculated using a group contribution method[43], decreased from 25.4 to 20.1 mN/m (open symbols in Fig. 1) with increasing number of fluorine atoms, eventually becoming smaller than γ_{PDMS} (Fig. 1). Following this trend, a series of fluoroacrylate homopolymers were synthesized to verify the experimental γ values. PTFEA, PPeFPA, and PHepFBA homopolymers were obtained *via* transesterification with a P*t*BA precursor using a method similar to that previously reported (Fig. S1)[16]. In γ evaluation, all 40 nm-thick homopolymer films were annealed at RT under vacuum for 1 d immediately before the measurements. Static CA values with DI water and ethylene glycol (Fig. S2) were measured to evaluate the γ values of PDMS and the fluoroacrylate homopolymers using the Owens–Wendt–Rabel–Kaelble method[44].

$$(1+\cos\theta_{solvent})\gamma_{solvent} = 2*\left(\sqrt{\gamma^d_{solvnet}\gamma^d_{polymer}} + \sqrt{\gamma^p_{solvnet}\gamma^p_{polymer}}\right) \quad (1)$$

where $\theta_{solvent}$ is the CA value of each solvent on the polymer surface, γ_i is the total surface tension of the *i*th component (namely, $\gamma_i = \gamma_i^d + \gamma_i^p$), and the superscript terms *d* and *p* denote the dispersion (or nonpolar) and polar components, respectively, of the surface tension. The experimentally determined γ_{PDMS} value of 21.1 mN/m (closed symbols in Fig. 1) is almost identical to that previously reported[42], and the γ values of the fluoro-

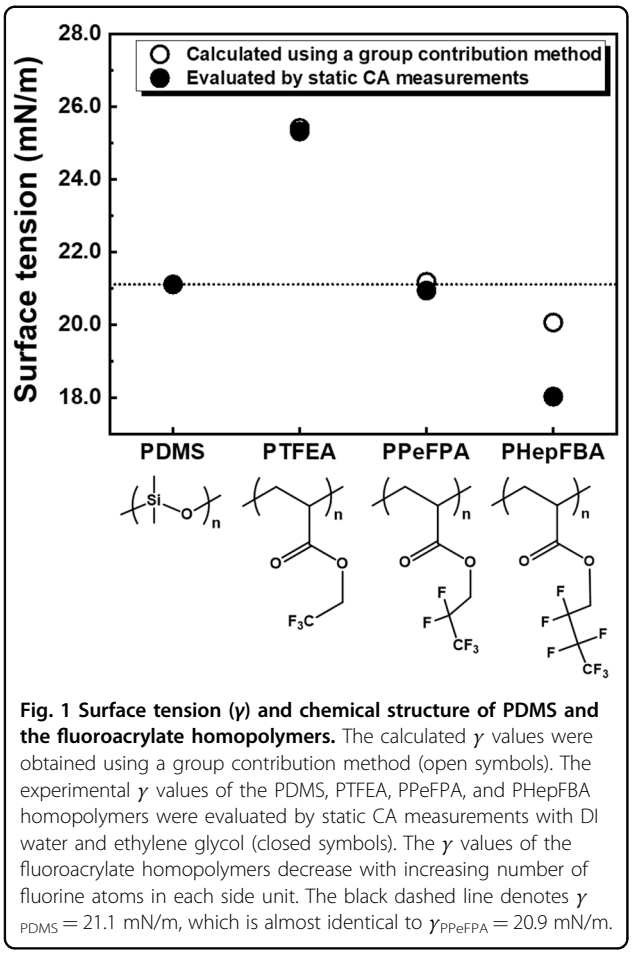

Fig. 1 Surface tension (γ) and chemical structure of PDMS and the fluoroacrylate homopolymers. The calculated γ values were obtained using a group contribution method (open symbols). The experimental γ values of the PDMS, PTFEA, PPeFPA, and PHepFBA homopolymers were evaluated by static CA measurements with DI water and ethylene glycol (closed symbols). The γ values of the fluoroacrylate homopolymers decrease with increasing number of fluorine atoms in each side unit. The black dashed line denotes $\gamma_{PDMS} = 21.1$ mN/m, which is almost identical to $\gamma_{PPeFPA} = 20.9$ mN/m.

acrylate homopolymers PTFEA, PPeFPA, and PHepFBA slightly decreased linearly (Table S1). In particular, $\gamma_{PPeFPA} = 20.9$ mN/m is remarkably close to γ_{PDMS}.

In pursuit of a new BCP with identical γ values of the two blocks, a lamella-forming PDMS-*b*-PPeFPA copolymer was synthesized *via* ATRP. The ATRP reaction was performed at 85 °C for 2 d in a purified Ar environment using PDMS-Br (macroinitiator)/PeFPA (monomer)/PMDETA (ligand)/CuBr (catalyst) in a molar ratio of 1.00:200:2.00:1.00 (Fig. 2a). Based on ^{1}H NMR analysis (Fig. S3a), M_n and f_{PPeFPA} were characterized to be 13,210 Da and 0.496, respectively. The molecular weight distribution was unimodal ($Đ < 1.10$), as determined by SEC (Fig. S3b). DSC analysis conducted at a rate of 30 °C/min (Fig. S3c) revealed that T_g of the PPeFPA block was −22.8 °C; however, T_g of the PDMS block (−122 °C)[45] could not be determined due to the instrument cooling limitations.

SAXS experiments were performed at the 4C beamline of the PAL, Korea. The PDMS-*b*-PPeFPA specimen was annealed and stored at RT, which is still above T_gs of the PDMS and PPeFPA blocks. 2D SAXS patterns were obtained while heating the BCP sample at a rate of 1.0 °C/min, and 1D intensity profiles were extracted from azimuthal integration of the 2D patterns over the scattering vector $q = (4\pi/\lambda)\sin\theta$, where 2θ and λ are the scattering angle and wavelength, respectively, of the incident X-ray. As shown in the SAXS intensity profile (Fig. 2b), an interlamellar spacing (L_0) of 17.3 nm was determined by $L_0 = 2\pi/q^*$, which is equivalent to a half-pitch feature size ($L_0/2$) of 8.7 nm. The intensity profile acquired at 30 °C exhibited higher-order peak positions of $q/q^* = 1:(2):3:(4):5$ relative to the primary reflection peak (q^*), characteristic of a lamellar structure, where the parentheses denote a loss of the even-numbered peaks. A TEM image (the inset of Fig. 2b) indicated a volume-symmetric lamellar structure with a feature size of 8.7 nm. As the temperature increased above the order-to-disorder transition (ODT) temperature of 235 °C, the intensity remarkably decreased to a broad maximum into a disordered state (Fig. S4a, b), indicating that thermally stable PDMS-*b*-PPeFPA could be obtained below the ODT temperature. Regarding the disordered state above the ODT, χ values between the PDMS and PPeFPA blocks (the inset of Fig. S4c) were extracted using the random phase approximation for incompressible BCP melts[11], where the SAXS intensity profiles were calibrated by a standard glassy carbon for normalization into the structure factor $S(q)$. A decrease in χ with increasing temperature (Fig. S4c) revealed $\chi = 9.6904/T + 0.0745$, although a fluctuation effect in the immediate vicinity of the ODT might result in underestimation.

PDMS-*b*-PPeFPA films were applied onto the substrates to investigate the microdomain orientation of the self-assembled nanostructure. An approximately $2.0L_0$ (~35-nm thick) PDMS-*b*-PPeFPA film was supported on a standard Si substrate with a 2 nm-thick native oxide layer and then annealed at RT under vacuum for 1 d. An SFM phase image (Fig. 2c) intentionally obtained at the film edge showed a hole–island lamellar morphology due to the incommensurability of the parallelly oriented lamellar microdomains. The top surface was dominated by the PPeFPA block since the experimental γ_{PPeFPA} value of 20.9 mN/m is slightly lower than $\gamma_{PDMS} = 21.1$ mN/m. Even nearly identical γ values of the PDMS and PPeFPA blocks could not entirely assist in directing the perpendicular lamellae. To demonstrate which block is more preferential with an oxide layer, ultrathin (≤10-nm thick) homopolymer films were spin-coated onto standard Si substrates and annealed at RT under vacuum for 7 d. Optical microscopy (OM) images (Fig. S5a) exhibited the dewetted structures of PDMS and PPeFPA homopolymer droplets. Based on the edge shapes probed by SFM height profile analysis (the inset of Fig. S5a), the average CA values of the dewetted PDMS and PPeFPA droplets were determined to be 25.8 ± 1.6° and 7.4 ± 0.8°, respectively, indicating that the preferential interactions with the thin

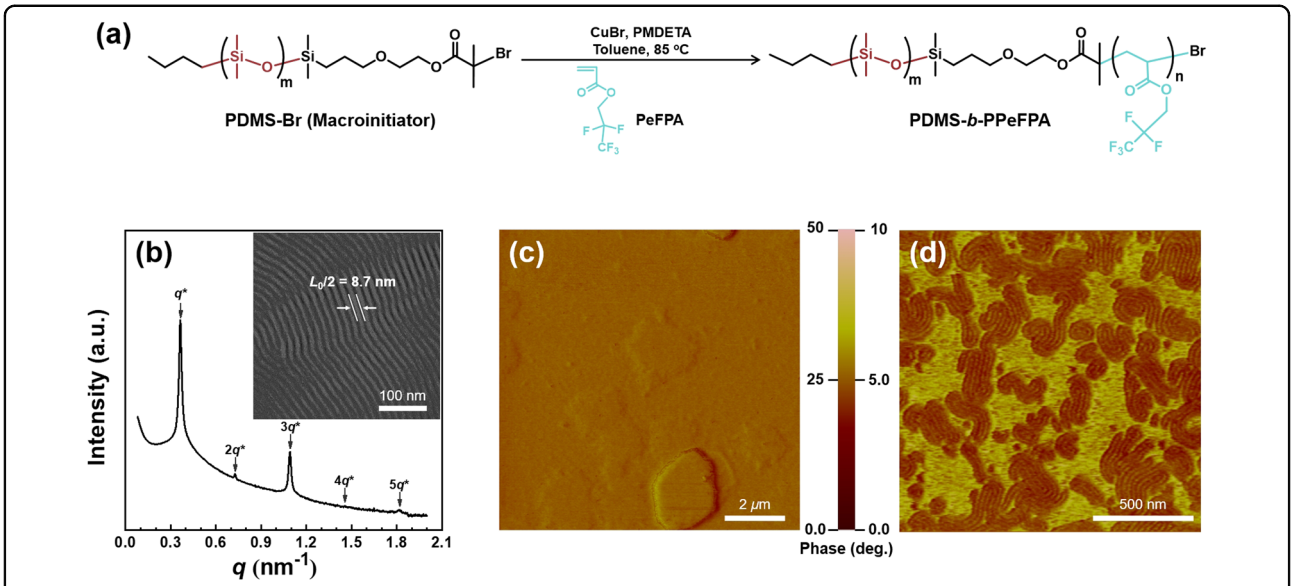

Fig. 2 Molecular design of PDMS-*b*-PPeFPA and morphological evaluation of the bulk and thin films. a ATRP scheme of the PDMS-*b*-PPeFPA copolymer using a PDMS-Br macroinitiator. **b** SAXS intensity profile of PDMS-*b*-PPeFPA measured at 30 °C. The higher-order peak positions of $q/q^* = 1:(2):3:(4):5$ with respect to q^* are characteristic of a volume-symmetric lamellar structure with $L_0 = 17.3$ nm. The inset TEM image corroborates the lamellar structure with a half-pitch feature size ($L_0/2$) of 8.7 nm. **c** SFM phase image of a $2.0L_0$ PDMS-*b*-PPeFPA film supported on a standard Si substrate with a 2 nm thick native oxide layer, displaying a hole–island lamellar morphology. **d** SFM phase image of a $2.0L_0$ PDMS-*b*-PPeFPA film supported on an H-passivated Si substrate, where the brightly colored regions represent the higher-T_g PPeFPA blocks. The partial fingerprint patterns and flat regions indicate the coexistence or mixed orientation of the perpendicular and parallel lamellae.

oxide layer were strong enough to propagate a parallel orientation of lamellar microdomains.

To suppress the preferential interactions with one block, the bottom interactions were converted from hydrophilic to hydrophobic; the thin oxide layer was removed by immersion in an aqueous HF solution (5 vol%; referred to as the H-passivated Si substrate). The CA value of the dewetted PDMS droplets on the H-passivated Si substrate decreased to 18.2 ± 0.8°, whereas that of the PPeFPA droplets increased to 17.1 ± 0.7° (Fig. S5b), maintaining weak preferential interactions with the PPeFPA block. The PDMS-*b*-PPeFPA film was supported on the H-passivated Si substrate and then annealed at RT under vacuum for 1 d. Interestingly, the partial fingerprint patterns in the SFM phase image (Fig. 2d) corresponded to the formation of perpendicular lamellae, while it coexisted with the other. From these results on the substrate interactions, we could understand that the bottom-substrate neutrality is more indispensable than the identical γ values of the two blocks for directing the perpendicular lamellae.

In regard to bottom-substrate neutrality, we adopted a physically adsorbed layer method that employs the same chemical identity[21]. The randomly adsorbed (or adhered) BCP chains controlled the interfacial properties toward the overlaid BCP films. The 30 nm-thick BCP films were annealed at RT under vacuum for 1 d to facilitate physisorption onto the H-passivated Si substrates. The films were thoroughly leached in *n*-heptane for 1 d to remove any unadsorbed chains, leaving approximately 4 nm-thick adsorbed layers on the substrates. The SFM phase (Fig. 3a) and height (Fig. S6a) images of the copolymer-adsorbed layer explicitly showed randomly distributed segregation because of the viscoelastic contrast between the PDMS and PPeFPA blocks, not likely the blocky interfaces between the two blocks.

To ascertain the distribution degree of the copolymer chains on the substrate, the correlation length (ξ) of the copolymer chains was determined by GISAXS experiments, which were performed at the 9 A beamline of PAL, Korea. In the 2D GISAXS geometry, $2\theta_f$ and α_f denote the exit angles of the X-ray beam along the *in-plane* ($q_{xy} = (4\pi/\lambda)\sin\theta_f$) and *out-of-plane* ($q_z = (2\pi/\lambda)\sin(\alpha_i + \alpha_f)$) directions, respectively, where α_i is the incident angle. The 2D GISAXS patterns were measured at $\alpha_i = 0.10°$, 0.12°, and 0.14°, and 1D intensity profiles (Fig. 3b) were scanned along the q_{xy}-direction at a constant α_f value to gain higher low-q intensities (scanned at $\alpha_f = 0.137°$ in the case of $\alpha_i = 0.12°$; the blue dashed line in the inset of Fig. 3b). The intensities were calibrated by subtracting the background scattering from the H-passivated Si substrate. The absence of a discernible Bragg peak scattered from the adsorbed layer of PDMS-*b*-PPeFPA indicated the formation of an intimately mixed phase on the substrate rather than a segregated periodic structure. Assumed as a nonparticulate two-phase system (PDMS and PPeFPA) that would be mixed irregularly[46], the correlation length (ξ) was evaluated using the

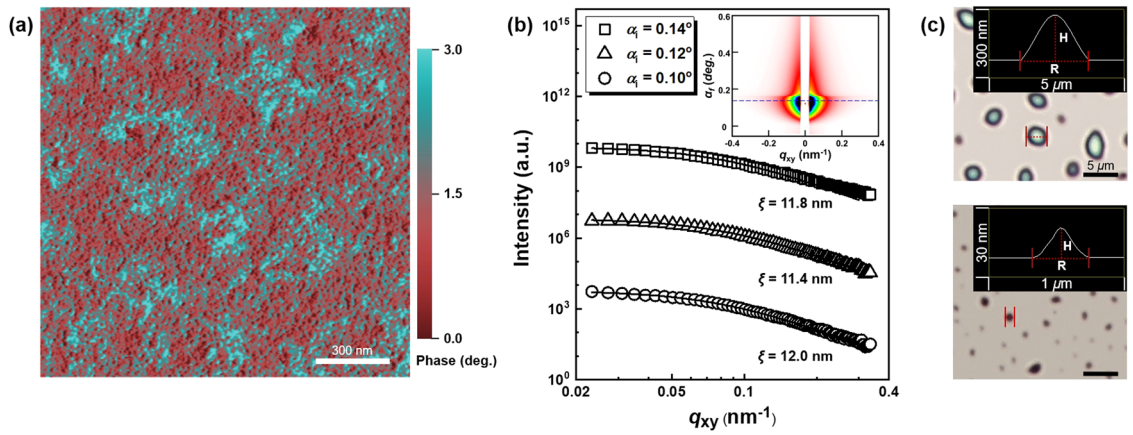

Fig. 3 Bottom-substrate neutrality of the physically adsorbed layer. a SFM phase image of the copolymer-adsorbed layer, which features randomly distributed chains of reddish PDMS and bluish higher-T_g PPeFPA blocks. **b** 1D intensity profiles scanned along the q_{xy}-direction at a constant α_f from the 2D GISAXS patterns at $\alpha_i = 0.10°$, 0.12°, and 0.14°. The intensity profiles are vertically shifted for clarity. The inset shows the 2D GISAXS pattern of the copolymer-adsorbed layer for $\alpha_i = 0.12°$, in which the blue dashed line represents the profile scanned at $\alpha_f = 0.137°$. The optimal fits generated using the Debye–Bueche model overlap the experimental results for $\alpha_i = 0.10°$, 0.12°, and 0.14°. **c** OM images of the dewetted PDMS (top) and PPeFPA (bottom) homopolymer droplets supported on the adsorbed layer. The insets show the SFM height profiles scanned across the dewetted droplets. The CA values of the dewetted homopolymer droplets are calculated using $\tan(\theta/2) = H/R$ (valid for $\theta \ll 90°$), where H and R denote the height and radius, respectively, of the droplets.

Debye–Buche model[47,48], as follows:

$$I(q) = \frac{C\xi^3}{\left(1+\xi^2 q^2\right)^2} \quad (2)$$

where C is a constant. An average value of $\xi \approx 11.7$ nm was produced from the optimal fit in the q-range of 0.023–0.300 nm^{-1} (Fig. 3b). This average ξ value for the adsorbed layer was considerably smaller than the inter-lamellar spacing of PDMS-*b*-PPeFPA ($L_0 = 17.3$ nm), indicating the compositional randomness of the copolymer chains on the substrate.

To demonstrate the effectiveness of the copolymer-adsorbed layers in controlling the surface energy, ultrathin (≤10 nm-thick) PDMS and PPeFPA homopolymer films were also spin-coated onto the same adsorbed layers. The homopolymer films annealed at RT under vacuum for 7 d generated dewetted structures of the PDMS and PPeFPA homopolymer droplets, as shown in the OM images (top and bottom parts of Fig. 3c, respectively). Investigated by SFM height profile analysis (the inset of Fig. 3c), the average CA values of the dewetted PDMS and PPeFPA droplets were determined to be 11.4 ± 0.4° and 4.9 ± 0.4°, respectively. Young's equation was employed to accurately assess the interfacial interaction ($\gamma_{i\text{-ads}}$) between each homopolymer and the adsorbed layer, as follows:

$$\gamma_{i-\text{ads}} = \gamma_{\text{ads}} - \gamma_i \cos\theta \quad (3)$$

where γ_{ads} and γ_i are the surface tensions of the adsorbed layer and homopolymers, respectively, and θ is the CA value of the dewetted homopolymer droplets on the adsorbed layer. γ_{ads} was evaluated as 22.6 mN/m using static CA measurements with DI water and ethylene glycol (Fig. S6b). From the average CA values of the PDMS and PPeFPA homopolymers (11.4° and 4.9°, respectively), the two interfacial interactions of $\gamma_{\text{PDMS-ads}}$ and $\gamma_{\text{PPeFPA-ads}}$ were evaluated to be 1.605 and 1.720 mN/m, respectively, which were nearly identical within the experimental error. These results collectively demonstrate the viability of our approach to utilizing physically adsorbed copolymer chains to screen the substrate interactions, producing the balanced interfacial interactions on the substrates. This strategy is analogous to the neutral-layer approach adopted for directing microdomains in BCP self-assembly[19,20].

PDMS-*b*-PPeFPA films were subsequently supported on the adsorbed layers by controlling the thickness from $1.0L_0$ to $3.0L_0$ and subsequently annealed at RT under vacuum for 1 d. Surprisingly, the SFM phase images (red box in Fig. 4a) displayed fingerprint patterns up to thicknesses of $2.3L_0$, which correspond to lamellar microdomains oriented perpendicular to the surface. A further increase in the thickness to $3.0L_0$ led to the emergence of several flat regions due to the presence of lamellar microdomains oriented parallel to the surface. The thickness window for mapping the perpendicular orientation suggests that the BCP films under dual neutral confinement successfully yielded lamellar microdomains oriented perpendicular to the interfaces. Above this window, parallel lamellae emerged due to the dissipation of substrate interactions because this is entropically more

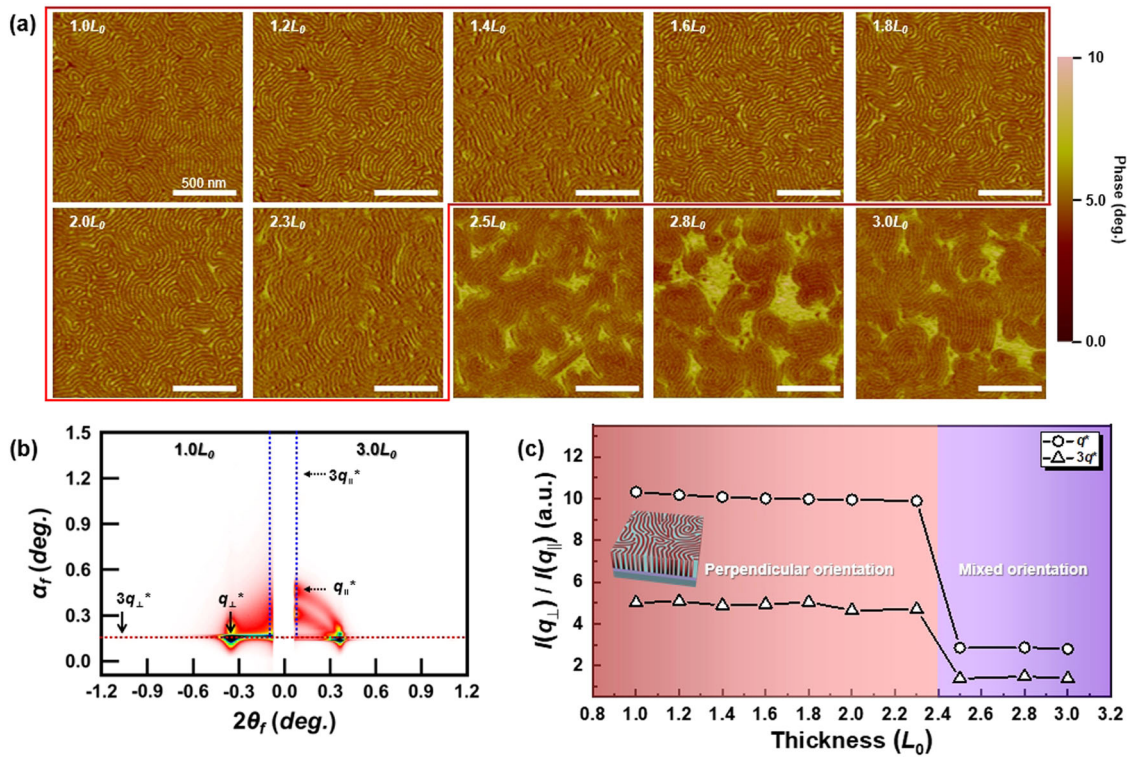

Fig. 4 1D directed assembly of BCP films supported on the adsorbed layers. a SFM phase images of PDMS-*b*-PPeFPA films supported on the adsorbed layers by controlling the thickness from $1.0L_0$ to $3.0L_0$, where the red box indicates the fingerprint patterns arising from the lamellar microdomains oriented perpendicular to the surface. **b** 2D GISAXS patterns of $1.0L_0$ (left) and $3.0L_0$ (right) PDMS-*b*-PPeFPA films supported on the adsorbed layers for $\alpha_i = 0.14°$. In the case of the $3.0L_0$ PDMS-*b*-PPeFPA film, the presence of both Bragg diffraction and an arc-shaped pattern validates the coexistence or mixed orientation of the perpendicular and parallel lamellae. **c** $I(q_\perp)/I(q_{||})$ as a function of the thickness. A higher $I(q_\perp)/I(q_{||})$ value indicates the presence of a larger population of perpendicular lamellae.

favorable than the formation of perpendicular lamellae[49]. In such a low-*N* PDMS-*b*-PPeFPA, the orientation of the lamellar microdomains could be determined by the entropic contribution associated with the molecular weight of BCP[50].

GISAXS experiments were also conducted at a constant $\alpha_i = 0.14°$, which is considerably higher than the critical angle of PDMS-*b*-PPeFPA films (0.109°), to trace the interior structure of the BCP films. The 2D GISAXS patterns of $1.0L_0$ and $3.0L_0$ PDMS-*b*-PPeFPA films (left and right parts of Fig. 4b, respectively) exhibited strong Bragg diffractions ($q_\perp{}^* = 0.357\ \mathrm{nm}^{-1}$) with higher-order peaks at $q/q_\perp{}^* = 1{:}3$, indicative of the perpendicular orientation of symmetric lamellae with $L_0 = 17.6$ nm. However, in regard to the $3.0L_0$ PDMS-*b*-PPeFPA film, the presence of both Bragg diffraction and an arc-shaped pattern demonstrated the coexistence or mixed orientation of the perpendicular and parallel lamellae. To quantify the thickness dependence of the microdomain orientation, the intensities were scanned along the q_{xy}-direction at $\alpha_f = 0.140°$ and along the q_z-direction at $2\theta_f = 0.090°$ (the red and blue dotted lines, respectively, in Fig. 4b and S7). Furthermore, the intensity ratio of $I(q_\perp)/I(q_{||})$ was analyzed as a function of the thickness because the $I(q_\perp)/I(q_{||})$ values are correlated with the populations of perpendicular to parallel lamellae (Fig. 4c). Relatively consistent values of $I(q_\perp)/I(q_{||})$ were observed with increasing thickness, which then abruptly decreased at $2.5L_0$, in agreement with the thickness-dependent SFM phase images (Fig. 4a).

To exploit the large dielectric contrast between the PDMS and PPeFPA homopolymers ($\Delta\varepsilon \approx 9.78$ at 100 Hz; Fig. S8a), the PDMS-*b*-PPeFPA films were subjected to a lateral E-field. A pair of electrodes with a 2 μm gap was prepared using parallel Au lines, and the copolymer-adsorbed layer was employed to achieve the bottom-substrate neutrality. Prior to the application of the lateral E-field, the $2.0L_0$ BCP film between the Au electrodes exhibited perpendicular lamellae owing to symmetric confinement with dual neutral interfaces, as shown in a top-view FE-SEM image (Fig. 5a). Being subjected to a direct current (DC) potential of 25 V/μm at RT for 0.5 h in an N_2 environment, the PDMS-*b*-PPeFPA film revealed an adaptively aligned orientation of perpendicular lamellae along the electric vector (Fig. 5b); however, several defects were inevitably formed due to the active chain

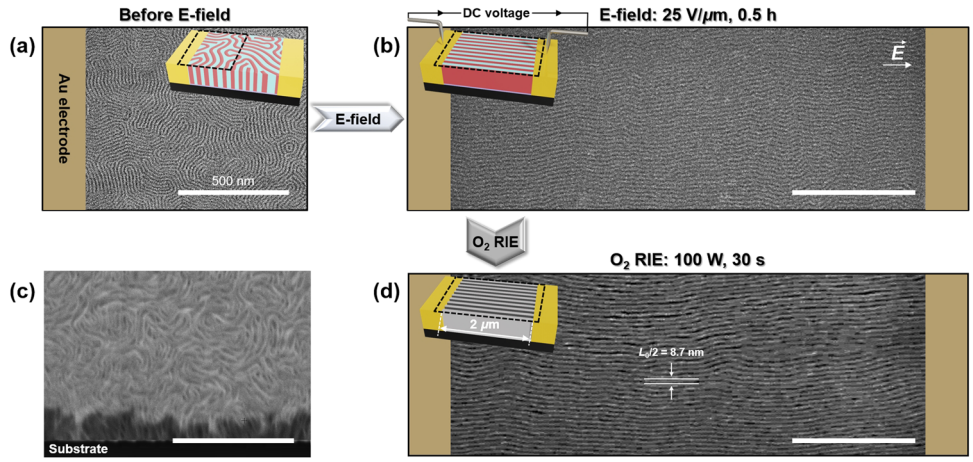

Fig. 5 2D directed assembly of BCP films with a lateral E-field and fabrication of air-inorganic nanoarrays through O_2 RIE. Top-view FE-SEM images of the $2.0L_0$ PDMS-*b*-PPeFPA films (**a**) near the parallel Au electrodes before applying the lateral E-field and (**b**) between the parallel Au electrodes with a 2 μm gap, at a DC potential of 25 V/μm at RT for 0.5 h in a N_2 environment. **c** Tilted-view FE-SEM image of the PDMS-*b*-PPeFPA film (**a**) after O_2 RIE. **d** Top-view FE-SEM image of the air–inorganic (oxidized PDMS) nanoarrays between the Au electrodes. The PDMS-*b*-PPeFPA film is subjected to a lateral E-field and then applied in O_2 RIE to produce unidirectionally aligned air-inorganic nanostructures emanating from the perpendicular lamellae.

mobility at RT. Notably, a short period (0.5 h) of E-field treatment at low temperatures was sufficient to enable unidirectional alignment of the perpendicular lamellae. This occurs because the large dielectric contrast between the PDMS and PPeFPA blocks was in synergy with rapid chain diffusion of the short segments.

Another advantage of using an inorganic–organic hybrid BCP film is that a high etch contrast is available during O_2 RIE. Remarkably, we identified that the etch contrast between the PDMS and PPeFPA homopolymers was approximately 2.5 times larger than that between the PS and poly(methyl methacrylate) homopolymers (Fig. S8b). The optimized O_2 RIE conditions were obtained at an RF power of 100 W for 30 s to thoroughly etch the organic PPeFPA block down, where the inorganic PDMS block was oxidized and remained intact with further etching. A tilted-view FE-SEM image (Fig. 5c) showed an air–inorganic structure obtained from the lamellae oriented perpendicular to the interfaces. Furthermore, O_2 RIE produced unidirectionally aligned air–inorganic (oxidized PDMS) nanoarrays (Fig. 5d) emanating from the perpendicular lamellae between the Au electrodes. Accordingly, the static CA value with DI water dramatically decreased from 91.5° to 22.5° upon O_2 RIE (Fig. S8c) because the hydrophobic methyl groups surrounding the Si–O backbone were transformed into hydrophilic polar silanol groups.

Conclusions

A new type of iso-γ, low-T_g, and silicon- and fluorine-containing BCP capable of room-temperature self-assembly was explored to secure the desired orientation of lamellar microdomains. With the essential condition that the air preferences of the two blocks should be identical to avoid the use of top-coat materials, an optimized PDMS-*b*-PPeFPA copolymer was selected and synthesized using an inorganic PDMS macroinitiator. A volume-symmetric lamellar structure with a half-pitch feature size of 8.7 nm was obtained, conforming with the high-χ and low-N characteristics. In terms of implementing the bottom-up substrate neutrality, the compositional randomness of the physically adsorbed BCP chains provided well-balanced interfacial interactions for the overlaid PDMS-*b*-PPeFPA ($\gamma_{\text{PDMS-ads}} \approx \gamma_{\text{PPeFPA-ads}}$), directing the lamellae to be oriented perpendicular to the interfaces at RT. As a result of the large dielectric contrast between the two blocks, the perpendicular lamellae were unidirectionally aligned along the electric vector within a short period (0.5 h) of E-field treatment at RT. Together with the remarkable etch contrast for O_2 RIE, we demonstrated unidirectional alignment of the air–inorganic (oxidized PDMS) perpendicular lamellae between the electrodes. Overall, this study showcases a system engineering approach not only for tailoring high-χ and low-N BCPs with identical γ values but also for aligning perpendicularly oriented lamellar microdomains, thus offering straightforward access to symmetric confinement with dual neutral interfaces in BCP films.

Acknowledgements

The authors acknowledge the NRF grants (2021R1A2C2006588, 2022R1A4A1020543, and 2019M1A2A2072417) funded by the Ministry of Science, ICT & Future Planning (MSIP), Korea.

Author details
[1]Department of Chemical and Biomolecular Engineering, Yonsei University, 50 Yonsei-ro, Seodaemun-gu, Seoul 03722, Korea. [2]Synchrotron Application Team, Pohang Accelerator Laboratory, 80 Jigok-ro, Nam-gu, Pohang 37673, Korea. [3]Soft Hybrid Materials Research Center, Korea Institute of Science and Technology, 5, Hwarang-ro 14-gil, Seongbuk-gu, Seoul 02792, Korea. [4]KU-KIST Graduate School of Converging Science and Technology, Korea University, 145 Anam-ro, Seongbuk-gu, Seoul 02841, Korea

Author contributions
S.J. and D.Y.R. conceived and executed the experiments. S.J., S.L., J.K., S.E., and W.H.N. obtained the experimental data. S.J., W.L., and J.G.S. analyzed the experimental results. D.Y.R. supervised the entire project. All authors contributed to the analysis and interpretation of the data in the manuscript.

Conflict of interest
The authors declare no competing interests.

Publisher's note
Springer Nature remains neutral with regard to jurisdictional claims in published maps and institutional affiliations.

Supplementary information The online version contains supplementary material available at https://doi.org/10.1038/s41427-023-00519-3.

Received: 5 August 2023 Revised: 11 November 2023 Accepted: 15 November 2023.
Published online: 29 December 2023

References

1. Schaller, R. R. Moore's law: past, present and future. *IEEE Spectr.* **34**, 52–59 (1997).
2. Harriott, L. R. Limits of lithography. *Proc. IEEE* **89**, 366–374 (2001).
3. Ito, T. & Okazaki, S. Pushing the limits of lithography. *Nature* **406**, 1027–1031 (2000).
4. Cho, J. H. et al. Printable ion-gel gate dielectrics for low-voltage polymer thin-film transistors on plastic. *Nat. Mater.* **7**, 900–906 (2008).
5. Maeda, R., Hayakawa, T. & Ober, C. K. Dual mode patterning of fluorine-containing block copolymers through combined top-down and bottom-up lithography. *Chem. Mater.* **24**, 1454–1461 (2012).
6. Hu, H., Gopinadhan, M. & Osuji, C. O. Directed self-assembly of block copolymers: a tutorial review of strategies for enabling nanotechnology with soft matter. *Soft Matter* **10**, 3867–3889 (2014).
7. Li, L. et al. Extreme ultraviolet resist materials for sub-7 nm patterning. *Chem. Soc. Rev.* **46**, 4855–4866 (2017).
8. Wang, Y. & Overmeyer, L. Chip-on-flex packaging of optoelectronic devices in polymer-based planar optical interconnects. *IEEE J. Sel. Top. Quantum Electron.* **24**, 1–8 (2018).
9. Ruiz, R. et al. Density multiplication and improved lithography by directed block copolymer assembly. *Science* **321**, 936–939 (2008).
10. Xiao, S. et al. Servo-integrated patterned media by hybrid directed self-assembly. *ACS Nano* **8**, 11854–11859 (2014).
11. Leibler, L. Theory of microphase separation in block copolymers. *Macromolecules* **13**, 1602–1617 (1980).
12. Sinturel, C., Bates, F. S. & Hillmyer, M. A. High χ–Low N Block Polymers: How Far Can We Go? *ACS Macro Lett.* **4**, 1044–1050 (2015).
13. Cushen, J. D. et al. Oligosaccharide/silicon-containing block copolymers with 5 nm features for lithographic applications. *ACS Nano* **6**, 3424–3433 (2012).
14. Nakatani, R. et al. Perpendicular orientation control without interfacial treatment of RAFT-synthesized high-χ block copolymer thin films with sub-10 nm features prepared via thermal annealing. *ACS Appl. Mater. Interfaces* **9**, 31266–31278 (2017).
15. Woo, S. et al. Molecular tailoring of poly (styrene-*b*-methyl methacrylate) block copolymer toward perpendicularly oriented nanodomains with sub-10 nm features. *ACS Macro Lett.* **6**, 1386–1391 (2017).
16. Jo, S., Jeon, S., Jun, T., Park, C. & Ryu, D. Y. Fluorine-containing styrenic block copolymers toward high χ and perpendicular lamellae in thin films. *Macromolecules* **51**, 7152–7159 (2018).
17. Lo, T.-Y., Krishnan, M. R., Lu, K.-Y. & Ho, R.-M. Silicon-containing block copolymers for lithographic applications. *Prog. Polym. Sci.* **77**, 19–68 (2018).
18. Matsen, M. Thin films of block copolymer. *J. Chem. Phys.* **106**, 7781–7791 (1997).
19. Mansky, P., Liu, Y., Huang, E., Russell, T. & Hawker, C. Controlling polymer-surface interactions with random copolymer brushes. *Science* 275, 1458–1460 (1997).
20. Ryu, D. Y., Shin, K., Drockenmuller, E., Hawker, C. J. & Russell, T. P. A generalized approach to the modification of solid surfaces. *Science* **308**, 236–239 (2005).
21. Lee, W. et al. Irreversible physisorption of PS-*b*-PMMA copolymers on substrates for balanced interfacial interactions as a versatile surface modification. *ACS Macro Lett.* **8**, 519–524 (2019).
22. Bates, C. M. et al. Polarity-switching top coats enable orientation of sub-10-nm block copolymer domains. *Science* **338**, 775–779 (2012).
23. Suh, H. S. et al. Sub-10-nm patterning via directed self-assembly of block copolymer films with a vapour-phase deposited topcoat. *Nat. Nanotechnol.* **12**, 575–581 (2017).
24. Lu, K.-Y. et al. Orienting silicon-containing block copolymer films with perpendicular cylinders via entropy and surface plasma treatment. *Macromolecules* **50**, 9403–9410 (2017).
25. Oh, J. et al. Universal perpendicular orientation of block copolymer microdomains using a filtered plasma. *Nat. Commun.* **10**, 2912 (2019).
26. Blachut, G. et al. A hybrid chemo-/grapho-epitaxial alignment strategy for defect reduction in sub-10 nm directed self-assembly of silicon-containing block copolymers. *Chem. Mater.* **28**, 8951–8961 (2016).
27. Oh, J. et al. Shear-rolling process for unidirectionally and perpendicularly oriented sub-10-nm block copolymer patterns on the 4 in scale. *ACS Nano* **15**, 8549–8558 (2021).
28. Amundson, K. et al. Effect of an electric field on block copolymer microstructure. *Macromolecules* **24**, 6546–6548 (1991).
29. Morkved, T. et al. Local control of microdomain orientation in diblock copolymer thin films with electric fields. *Science* **273**, 931–933 (1996).
30. Olszowka, V., Kuntermann, V. & Böker, A. Control of orientational order in block copolymer thin films by electric fields: a combinatorial approach. *Macromolecules* **41**, 5515–5518 (2008).
31. Olszowka, V. et al. Electric field alignment of a block copolymer nanopattern: direct observation of the microscopic mechanism. *ACS Nano* **3**, 1091–1096 (2009).
32. Ruppel, M. et al. Electric field induced selective disordering in lamellar block copolymers. *ACS Nano* **7**, 3854–3867 (2013).
33. Kathrein, C. C. et al. Combining graphoepitaxy and electric fields toward uniaxial alignment of solvent-annealed polystyrene–*b*–poly (dimethylsiloxane) block copolymers. *Chem. Mater.* **27**, 6890–6898 (2015).
34. Jeon, H. U. et al. Electric field directed self-assembly of block copolymers for rapid formation of large-area complex nanopatterns. *Mol. Syst. Des. Eng.* **2**, 560–566 (2017).
35. Pester, C. W., Liedel, C., Ruppel, M. & Böker, A. Block copolymers in electric fields. *Prog. Polym. Sci.* **64**, 182–214 (2017).
36. Jo, S. et al. Balanced interfacial interactions for fluoroacrylic block copolymer films and fast electric field directed assembly. *Chem. Mater.* **32**, 9633–9641 (2020).
37. Jeon, H. I. et al. Repairable macroscopic monodomain arrays from block copolymers enabled by photoplastic and photodielectric effects. *ACS Nano* **17**, 8367–8375 (2023).
38. Segalman, R. A. Patterning with block copolymer thin films. *Mater. Mater. Sci. Eng. R* **48**, 191–226 (2005).
39. Gu, X., Gunkel, I. & Russell, T. P. Pattern transfer using block copolymers. *Philos. Trans. R. Soc., A* **371**, 20120306 (2013).
40. Jung, Y. S. & Ross, C. A. Orientation-controlled self-assembled nanolithography using a polystyrene−polydimethylsiloxane block copolymer. *Nano Lett.* **7**, 2046–2050 (2007).
41. Jeon, S. et al. Frank–Kasper phases identified in PDMS-*b*-PTFEA copolymers with high conformational asymmetry. *Macromol. Rapid Commun.* **40**, 1900259 (2019).
42. Brandrup, J., Immergut, E. H., Grulke, E. A., Abe, A. & Bloch, D. R. *Polymer Handbook* (Wiley, 1999).
43. Van, K. D. *Properties of Polymers* (Elsevier, 1976).
44. Wu, S. *Polymer Interface and Adhesion* (Routledge, 2017).

45. Aranguren, M. I. Crystallization of polydimethylsiloxane: effect of silica filler and curing. *Polymer* **39**, 4897–4903 (1998).
46. Roe, R.-J. *Methods of X-ray and Neutron Scattering in Polymer Science* (Oxford University Press, 2000).
47. Debye, P. & Bueche, A. Scattering by an inhomogeneous solid. *J. Appl. Phys.* **20**, 518–525 (1949).
48. Debye, P., Anderson, H. Jr & Brumberger, H. Scattering by an inhomogeneous solid. II. The correlation function and its application. *J. Appl. Phys.* **28**, 679–683 (1957).
49. Pickett, G., Witten, T. & Nagel, S. Equilibrium surface orientation of lamellae. *Macromolecules* **26**, 3194–3199 (1993).
50. Choi, S. et al. Lamellar microdomain orientation and phase transition of polystyrene-*b*-poly (methyl methacrylate) films by controlled interfacial interactions. *Soft Matter* **8**, 3463–3469 (2012).